Journal of Asian Earth Sciences 87 (2014) 69–78

Contents lists available at ScienceDirect

Journal of Asian Earth Sciences

journal homepage: www.elsevier.com/locate/jseaes

LA-ICP-MS zircon geochronology and platinum-group elements characteristics of the Triassic basalts, SW China: Implications for post-Emeishan large igneous province magmatism

Jiawei Zhang [a,b], Zhilong Huang [a,*], Taiyi Luo [a], Zaifei Yan [a]

[a] State Key Laboratory of Ore Deposit Geochemistry, Institute of Geochemistry, Chinese Academy of Sciences, Guiyang 550002, China
[b] University of Chinese Academy of Sciences, Beijing 100049, China

ARTICLE INFO

Article history:
Received 31 October 2013
Received in revised form 18 February 2014
Accepted 24 February 2014
Available online 3 March 2014

Keywords:
Platinum-group elements
Geochronology
Low-degree partial melting
Basalts
Emeishan large igneous province
SW China

ABSTRACT

The Triassic post-Emeishan large igneous province (ELIP) basalts, mainly found in the Kaiyuan (KY), Qilinshan (QLS), and Laochang–Kafang (LK) areas, show spatial and geochemical relationships with the Permian ELIP, SW China. Specifically, the post-ELIP basalts are located in the southern part of the intermediate zone of the ELIP. These basalts have major trace element and Sr–Nd isotope features that are similar to those of Permian Emeishan high-Ti basalts. The LA-ICP-MS zircon U–Pb age and whole-rock platinum-group elements (PGE) concentrations of the post-ELIP basalts are reported in this paper. The determined age of 247.7 ± 1.4 Ma for the KY volcanic rocks is almost 10 Ma younger than the termination age of the ELIP magmatism, supporting their origin from post-ELIP magmatism. All the post-ELIP basalts show uniform but significant low PGE contents. Ir and Ru are depleted relative to Rh, Pt, and Pd in the primitive mantle-normalized PGE patterns, suggesting that a low degree of partial melting of the mantle source plays an important role in the PGE characteristics of the post-ELIP basalts. The Ir and Ru contents of the post-ELIP basalts are similar to those of the Emeishan high-Ti basalts. However, the Pt and Pd contents are strikingly depleted. This is consistent with the notion of early extraction of palladium-group PGE during the eruption of the Emeishan basalts.

1. Introduction

The Emeishan large igneous province (ELIP) is located along the western margin of the Yangtze block in SW China (Fig. 1a) and covers an area of 250,000 km^2 (Chung and Jahn, 1995). The ELIP is considered to be one of the best examples of a mantle plume-generated large igneous province (LIP) (e.g., Xu et al., 2001, 2004). Various mafic and felsic rocks—mainly continental flood basalts, mafic intrusions, and picritic basalts—have been recognized to be associated with the ELIP. Based on previous petrological studies, the Emeishan flood basalts have been classified chemically into two major magma types: high-Ti and low-Ti basalts. The high-Ti basalts are characterized by TiO_2 contents over 2.5 wt.% and Ti/Y ratios over 500. They are the dominant magma type in the periphery of the ELIP (Xu et al., 2004).

The age of the ELIP (around 260 Ma) has been firmly confirmed by U–Pb analyses on zircons from the mafic and alkaline intrusions (e.g., Zhou et al., 2002; He et al., 2007; Shellnutt et al., 2012). The zircons inherited felsic extrusives in the uppermost Emeishan lava in the lowermost Xuanwei Formation, which yielded ages of 257 ± 3 and 260 ± 5 Ma, placing constraints on the absolute termination age of the Emeishan volcanism (He et al., 2007). Shellnutt et al. (2012) used a higher precision chemical abrasion thermal ionization mass spectrometry (CA-TIMS) method to date the intrusive rocks of the Panxi region of the ELIP, finding that plume-related magmatism was likely to have been short-lived (of the order of 2 Ma) and must have ended by 257 Ma.

Meanwhile, recent studies have suggested a late-stage magmatism in the ELIP. The Triassic basalts in the southern ELIP were mainly found in the Kaiyuan (KY), Qilinshan (QLS), and Laochang–Kafang (LK) areas, which are located in the southern part of the intermediate zone of the ELIP (Fig. 1a), and have major trace element and Sr–Nd isotope features that are similar to those of Permian Emeishan high-Ti basalts. However, these basalts yield an age of 248.2 ± 6.1 Ma (Zhang et al., 2013), which is 10 Ma younger than the termination age of ELIP magmatism. Consequently, Zhang et al. (2013; unpublished results) have suggested that these basalts could be a proxy for post-ELIP magmatism. These basalts are pivotal because they can provide valuable information about

* Corresponding author. Tel.: +86 851 5895900; fax: +86 851 5891664.
E-mail address: huangzhilong@vip.gyig.ac.cn (Z. Huang).

http://dx.doi.org/10.1016/j.jseaes.2014.02.023
1367-9120/

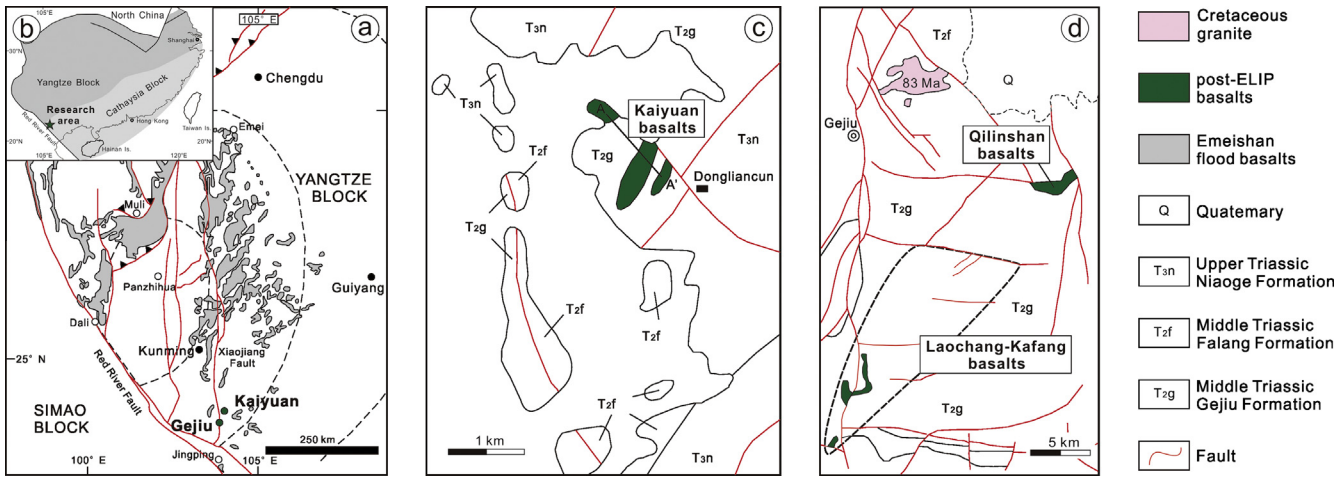

Fig. 1. (a) Simplified tectonic map showing the study area in relation to South China's major tectonic units (Li et al., 2007). (b) Simplified map showing the Emeishan basalt outcrop and dashed curves separate inner, intermediate and outer zones of dome, which are characterized by varying extent of erosion of Maokou limestone, base on Xu et al. (2004). (c) The geological map of Kaiyuan area. (d) The geological map of Gejiu area.

the source of post-ELIP magmatism. However, previous dating results are less precise and need to be tested by further investigation.

Platinum-group elements (PGE: Os, Ir, Ru, Rh, Pt, and Pd) are highly siderophile elements that can provide information on the petrogenesis of mantle-derived igneous rocks and their source. They are potential tracers of these mantle petrogenetic processes because these elements are very sensitive to the extent of melting, magma–rock interaction, sulfur saturation, and sulfide segregation (Barnes et al., 1985; Keays, 1995; Lorand et al., 2008). Recently, PGE studies focused on basalts and picrites from the ELIP have been well reported (Wang et al., 2007; Qi et al., 2008; Qi and Zhou, 2008; Song et al., 2008, 2009; Li et al., 2012). However, thus far PGE studies of the post-ELIP basalts have been lacking.

Therefore, in this paper we report new and precise LA-ICP-MS zircon U–Pb age and PGE contents of the post-ELIP basalts. The geochronological work aims at further constraining the precise age of the post-ELIP magmatism. The PGE data combined with previous studies for the post-ELIP basalts could provide an opportunity to evaluate the roles of mantle melting, crystal fractionation, and crustal contamination in controlling the PGE distribution in these rocks and, more significantly, to understand how the PGE contents will change in the residual mantle and in its remelt products after the Emeishan main plume event.

2. Geological background

South China is composed of two major blocks: the Yangzte block and Cathaysia block, respectively. The closure of the ocean between the Yangtze block and the Cathaysia block occurred between approximately 1000 and 900 Ma (e.g., Li et al., 2007). Plume related basaltic trap volcanism (ELIP) began on the southwest margin of the Yangtze craton at 260 Ma and ended at 257 Ma (Shellnutt et al., 2012). The Triassic post-ELIP basalts are scattered throughout the Bapanzhai and Dongliancun, Kaiyuan area, and are widely discovered at Qilinshan, Laochang, and Kafang, Gejiu tin-polymetallic ore district (YBGMR, 1982; Xue, 2002; Zhang et al., 2013), and the Funing area southeastern Yunnan province, China (YBGMR, 1982). Tectonically, this district is located at the westernmost end of the Cathaysia block, being adjacent to the Yangtze block in the north and to the Red River fault in the south (Fig. 1b). Simultaneously, this area is located at the southern part of the intermediate zone of the ELIP (Xu et al., 2004). It was suggested that these basaltic lavas formed in an extensional tectonic setting (rift) within the Yangtze craton (Zheng and Liu, 1993; Xue, 2002; Luo et al., 2008). This intraplate environment was also indicated by the paleogeographic reconstructions of Metcalfe (2006). The Late Permian Emeishan basalts are found in both eastern Kaiyuan and northwestern Gejiu. No picrites have been found in the Kaiyuan–Gejiu area (YBGMR, 1982).

The Middle Triassic Gejiu Formation (T_2g) and the Falang Formation are the dominant strata (over 3000 m). These basaltic lavas are conformably interbedded within the Gejiu Formation. The KY basalts are subdivided into three units with intercalated sedimentary rocks according to their petrographic characteristics (Fig. 2a). The KY basalts are dark-green and dark-brown, with massive and amygdaloidal structure, the amygdaloids are filled with calcites. The major rock forming minerals include clinopyroxene, alkali feldspar and Fe–Ti oxides. The interlayer dark-red basaltic andesite is conformable contact with the basalt, as evident from the outcrop of the KY area (Fig. 2b–d). The QLS basalts are dark-green, with amygdaloidal structure. The amygdaloids are 0.2–2 cm in across and asymmetrical and display a preferred orientation. The amygdaloids are primarily composed of chalcedony with manifold sharp edges and asymmetry textures. The groundmass is primarily composed of oriented alkali feldspar, fine grained clinopyroxene and Fe–Ti oxides. The LK basalts are primarily dark-green or dark-gray in color and were overprinted by strong deuteric alteration. The basalts are primarily massive, but amygdaloidal structure is also present. The schistosity is extensively developed, and the primary textures are intergranular and intersertal textures. The alteration minerals in the basalts primarily consist of phlogopite, chlorite, actinolite, tremolite and biotite. The accessory minerals included ilmenite, magnetite, apatite and sulfides. Besides the differences in petrologic feature, these basalts have major trace element and Sr–Nd isotope features that are similar to those of Permian Emeishan high-Ti basalts. Specifically, these basalts are all alkaline, high Ti ($TiO_2 > 2.5$ wt.%) basalts, with OIB-like trace element ratios. The $\varepsilon Nd(t)$ values of these basalts ranging from −2.2 to 2.5 and the $(^{87}Sr/^{86}Sr)_i$ values ranging from 0.70424 to 0.70637. The plot of the Sr–Nd isotopic compositions of these basalts display a negative correlation with that of the mantle array and overlap with that of the Emeishan flood basalts (Zhang et al., 2013; unpublished results).

The Late Cretaceous igneous rocks were emplaced in the Gejiu district within a short period, from 76 to 85 Ma, rock types include equigranular and porphyritic granites, gabbro and nepheline syenite (Cheng and Mao, 2010). The LK basalts exhibit a close spatial

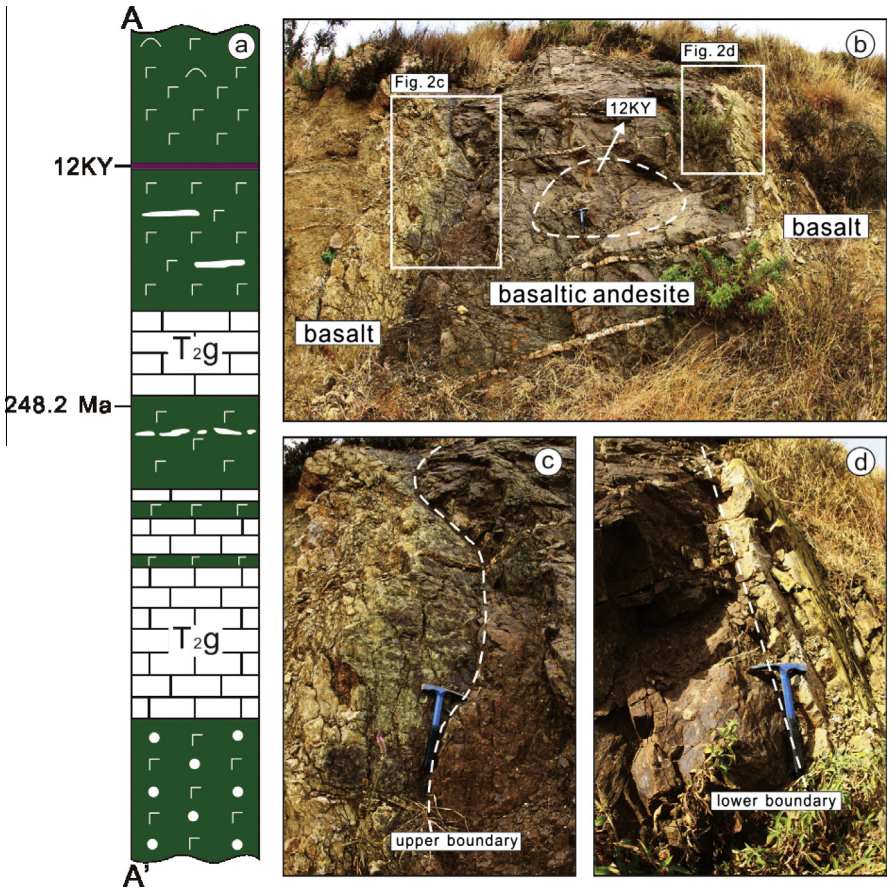

Fig. 2. (a) Composite stratigraphic column of the KY basalt measured section. (b) The outcrop of chronological sample 12KY. (c) The upper boundary between KY basalt and basaltic andesite. (d) The lower boundary between KY basalt and basaltic andesite.

association to the Late Cretaceous Laochang granites. Therefore, they have suffered strong late-stage alteration, sulfide mineralization, and dolomite wall-rock alteration. The main altered mineral of the LK basalts is phlogopite. Zhang et al. (2012) reported a phlogopite ^{40}Ar–^{39}Ar plateau age (85 ± 0.6 Ma) for the LK basalts. The phlogopite ^{40}Ar–^{39}Ar plateau altered age of the LK basalts is consistent with the zircon U–Pb age of the Laochang granites (83.3–85.5 Ma), indicating that the alteration of LK basalts was temporally related to the emplacement of the Late Cretaceous granite.

3. Analytical methods

3.1. Zircon LA-ICP-MS U–Pb dating

The 12KY basaltic andesite sample from the Kaiyuan section was selected for geochronological study (Fig. 2a). For cathodoluminescent (CL) imaging, representative zircon grains were handpicked and mounted in epoxy resin disks and subsequently polished and coated with carbon. The internal morphology was examined using CL prior to U–Pb isotopic analysis.

U–Pb geochronology of zircons was conducted by LA-ICP-MS at the State Key Laboratory of Ore Deposit Geochemistry, Institute of Geochemistry, Chinese Academy of Sciences, Guiyang. A GeoLasPro laser-ablation system (Lamda Physik, Gottingen, Germany) and an Agilent 7700x ICP-MS (Agilent Technologies, Tokyo, Japan) were combined for the experiments. The 193-nm ArF excimer laser, homogenized by a set of beam delivery systems, was focused on the zircon surface with a fluence of 10 J/cm^2. The ablation protocol employed a spot diameter of 32 μm at 5 Hz repetition rate for 40 s (equating to 200 pulses). Helium was applied as a carrier gas to efficiently transport the aerosol to the ICP-MS. Zircon 91500 was used as an external standard to correct for instrumental mass discrimination and elemental fractionation. Zircon GJ-1 and Plešovice were treated as quality control for geochronology. Raw data reduction was performed off-line with ICPMSDataCal software (Liu et al., 2010a,b). The age computations and concordia diagrams were made using ISOPLOT (version 3.0) (Ludwig, 2003). The errors quoted in the tables and figures were at the 1σ level, and the weighted average ages were calculated at the 2σ level.

3.2. Whole-rock PGE compositions

The PGE concentrations were measured by isotope dilution (ID)-ICP-MS in the State Key Lab of Ore Deposit Geochemistry, Institute of Geochemistry, Chinese Academy of Sciences, Guiyang, following a modified method reported by Qi et al. (2011). Ten grams of powdered sample and appropriate amounts of the enriched isotope spike solution were carefully weighed and placed in a 120 ml PTFE beaker to remove silicates. After the beaker was sealed in a stainless steel pressure bomb, the dried residue was then digested with HF + HNO_3 at 190 °C for about 24 h. The eluted solution was evaporated to 2–3 ml and then transferred to a 15 ml centrifuging tube for ICP-MS measurement after chemical preparation. The blank levels (in nanograms), detection limits (DL, in nanograms per gram), and analytical results for reference materials are listed in Table 1. The average compositions of the five total procedural reagent blanks ranged from 0.008 ng (Ru) to 0.033 ng (Pd) and the detection limits ranged from 0.004 ng/g (Ir) to 0.014 ng/g

Table 1
Blank level (ng), detection limits (DL, ng/g) and analytical results (ng/g) for reference materials.

Elements	Blank	DL (3σ)	UMT-1		WPR-1		WGB-1		TDB-1	
			Certified	Measured	Certified	Measured	Certified	Measured	Certified	Measured
Ir	0.009	0.004	8.8	8.21	13.5	17.0	0.3	0.16	0.15[a]	0.11
Ru	0.008	0.008	10.9	9.82	22	23.3	0.3	0.12	0.3[a]	0.6
Rh	0.009	0.006	9.5	9.54	13.4	12.9	0.32	0.22	0.7[a]	0.51
Pt	0.021	0.014	128	120	285	290	6.1	5.39	5.8 ± 1.1	4.90
Pd	0.033	0.012	106	113	235	277	13.9	13.8	22.4 ± 1.4	22.6

Note: The detection limit (ng/g) is calculated as three times the standard deviation of five individual procedural reagent blanks (ng), divided by the sample mass. The certified values were followed Govindaraju (1994).
[a] Provisional values.

(Pt). The analytical results for the reference standards UMT-1, WPR-1, WGB-1 and TDB-1 were in excellent agreement with the certified values.

3.3. Whole-rock S compositions

Whole-rock S compositions were determined by Elementar vario MACRO cube at the State Key Laboratory of Environmental Geochemistry, Institute of Geochemistry, Chinese Academy of Sciences, Guiyang. A total of 20 mg from each sample was weighed in tin vessels and loaded into the integrated carousel. Catalytic combustion was carried out at a permanent temperature of up to 1200 °C. The formed analyte SO_2 gas mixtures were separated into their components via purge and trap chromatography and then detected by using a thermal conductivity detector (TCD). The detection range for S was 0–18 mg and the standard deviation was less than 0.2%.

4. Analytical results

4.1. Zircon LA-ICP-MS U–Pb age

The zircon LA-ICP-MS U–Pb dating results are listed in Table 2. The zircons are 50–100 μm in size and exhibit euhedral appearances with dark but visible magmatic oscillatory zoning. Inclusions, cores, and cracks are absent, as shown in the CL images (Fig. 3a). Sixteen analyses were made and all results fell within a single population of 247–248 Ma. The measurements formed a cluster on the concordia plot with a weighted mean $^{206}Pb/^{238}U$ age of 247.7 ± 1.4 Ma (MSWD = 0.015) (Fig. 3b). The zircons have a relatively wide range in Th (606–1398 ppm) and U (993–1614 ppm) contents, with Th/U ratios ranging from 0.57 to 0.87 (Table 2).

The new LA-ICP-MS dating result gives a more precise age of 247.7 ± 1.4 Ma for the post-ELIP KY basaltic andesite, although it is consistent with our previous work for the KY basalts (248.2 ± 6.1 Ma) within uncertainty (Fig. 2a). Thus, it is suggested that the KY basalts formed at ~248 Ma, almost 10 Ma younger than the termination age of ELIP magmatism. This observation confirms that the KY, QLS, and LK basalts are a proxy for the post-ELIP magmatism, as proposed by Zhang et al. (2013; unpublished results).

4.2. PGE abundances in whole rocks

The concentrations of Ni, Cu, and PGE in the post-ELIP basalts are listed in Table 3. The PGE concentrations in all samples are above the detection limits. The post-ELIP basalts have low PGE concentrations. The KY basalts have Ir, Ru, Rh, Pt, and Pd contents of 0.062–0.120, 0.094–0.163, 0.050–0.096, 0.779–1.812, and 0.927–3.283 ppb, respectively; the QLS basalts have Ir, Ru, Rh, Pt, and Pd contents of 0.045–0.093, 0.037–0.148, 0.020–0.059, 0.314–0.759, and 0.560–1.172 ppb, respectively; and the LK basalts have Ir, Ru, Rh, Pt, and Pd contents of 0.042–0.112, 0.060–0.152, 0.023–0.048, 0.280–0.649, and 0.582–3.826 ppb, respectively.

Fig. 6a–c illustrates the primitive mantle–normalized patterns of Ni, Cu, and PGE for the post-ELIP basalts. The losses on ignition (LOI) of the post-ELIP basalts were relatively high and the LK basalt had suffered strong hydrous fluids alteration and sulfide mineralization (Zhang et al., unpublished results). However, the primitive mantle–normalized PGE patterns of the post-ELIP basalts are very uniform, indicating that the PGE of the post-ELIP basalts remained immobile during the process of physical and chemical alteration.

Table 2
U–Pb isotopic data for zircons from the Kaiyuan volcanic rocks.

Sample	Pb ppm	Th ppm	U ppm	Th/U Ratio	$^{207}Pb/^{235}U$ Ratio	$^{207}Pb/^{235}U$ 1 sigma	$^{206}Pb/^{238}U$ Ratio	$^{206}Pb/^{238}U$ 1 sigma	$^{207}Pb/^{235}U$ Age (Ma)	$^{207}Pb/^{235}U$ 1 sigma	$^{206}Pb/^{238}U$ Age (Ma)	$^{206}Pb/^{238}U$ 2 sigma
12KY01	66.6	827	1272	0.65	0.26489	0.00699	0.03913	0.00041	238.6	5.6	247.4	2.6
12KY02	52.1	663	993	0.67	0.26386	0.00706	0.03922	0.00041	237.8	5.7	248.0	2.5
12KY03	64.0	864	1188	0.73	0.26616	0.00587	0.03925	0.00039	239.6	4.7	248.2	2.4
12KY04	52.9	684	1064	0.64	0.25511	0.00633	0.03913	0.00041	230.7	5.1	247.4	2.5
12KY05	90.8	1398	1614	0.87	0.27084	0.00656	0.03911	0.00050	243.4	5.2	247.3	3.1
12KY06	78.7	1216	1410	0.86	0.27839	0.00728	0.03910	0.00049	249.4	5.8	247.2	3.1
12KY07	66.1	927	1273	0.73	0.25808	0.00554	0.03912	0.00044	233.1	4.5	247.4	2.7
12KY08	69.9	1013	1288	0.79	0.27488	0.00729	0.03920	0.00052	246.6	5.8	247.9	3.2
12KY09	55.2	665	1133	0.59	0.27861	0.00693	0.03928	0.00046	249.6	5.5	248.4	2.8
12KY10	55.4	689	1143	0.60	0.27804	0.00721	0.03916	0.00046	249.1	5.7	247.6	2.9
12KY11	65.5	937	1263	0.74	0.27020	0.00630	0.03918	0.00046	242.9	5.0	247.7	2.8
12KY12	59.7	765	1227	0.62	0.28120	0.00709	0.03918	0.00047	251.6	5.6	247.8	2.9
12KY13	49.4	606	1055	0.57	0.26712	0.00750	0.03913	0.00050	240.4	6.0	247.4	3.1
12KY14	57.3	872	1068	0.82	0.28969	0.00743	0.03911	0.00047	258.3	5.8	247.3	2.9
12KY15	74.2	1133	1388	0.82	0.27538	0.00718	0.03913	0.00043	247.0	5.7	247.5	2.7
12KY16	60.5	845	1154	0.73	0.26883	0.00870	0.03919	0.00052	241.8	7.0	247.8	3.2

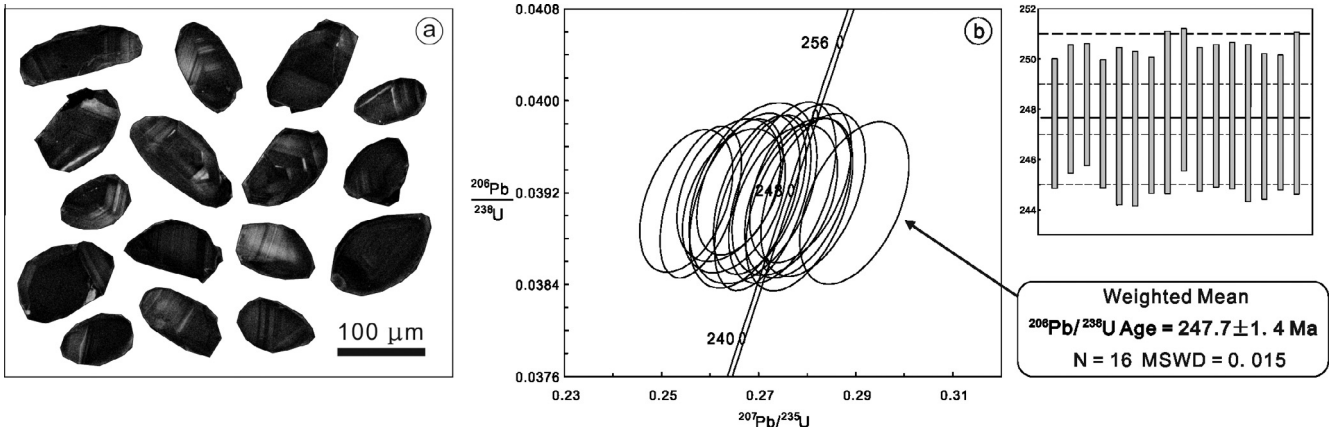

Fig. 3. (a) The cathodoluminescence images for the zircons from sample 12KY for LA-ICP-MS dating. (b) The U–Pb concordia plots showing results of LA-ICP-MS dating of zircons.

Therefore, the concentrations of PGE reported here are assumed to represent suitable proxies for evaluating the petrogenesis.

PGE are traditionally subdivided into iridium-group PGE (IPGE; Ir and Ru) and palladium-group PGE (PPGE; Rh, Pd, and Pt). Positive correlations were found between PPGE and IPGE in the samples (not shown). All the post-ELIP basalts display depletion of the IPGE relative to the PPGE in the primitive mantle–normalized PGE patterns. When compared with the representative Emeishan high-Ti basalts, the IPGE contents of the post-ELIP basalts are similar to the Emeishan high-Ti basalts. However, the PPGE contents are strikingly depleted. All the samples show a positive Ru anomaly relative to Ir and Rh.

4.3. S abundances in whole rocks

The S concentrations of the post-ELIP basalts are listed in Table 3. The S contents of KY are low and uniform, ranging from 130 to 340 ppm, with an average of 174 ppm. The S contents of QLS are also low and uniform, ranging from 150 to 330 ppm, with an average of 229 ppm. However, the S contents of LK basalts exhibit a very large range, from 370 to 3460 ppm; no correlations between PGE concentrations and S contents are observed.

5. Discussion

5.1. Lack of sulfide segregation during fractional crystallization and crustal contamination

Because of the very large immiscible sulfide liquid/silicate melt partition coefficient ($D_{Sul/Sil}$) (1500–4700 for Ir, 1200–4100 for Ru, 1100–6900 for Pt, and 1200–6300 for Pd, according to Fleet et al., 1999), the sulfide is an extremely potent agent for the collection and segregation of PGE from magmas. It has been suggested that a very small degree of sulfide segregation can result in significant PGE depletion (Lightfoot and Keays, 2005).

The whole-rock Cr content could be a good fractionation index for the Emeishan flood basalts (Wang et al., 2007). The presences of clinopyroxene phenocrysts in most post-ELIP samples supports early crystallization of this mineral (Zhang et al., 2013, unpublished results). Meanwhile, a positive correlation exists between Cr contents and whole-rock MgO contents (Fig. 5a), suggesting that the post-ELIP basalts had experienced fractional crystallization prior to the lava eruption.

Sulfur is a strongly incompatible element during fractional crystallization because it does not enter any of the common fractionating solid phases in cooling silicate magma (e.g., Keays, 1995). Its concentration increases with progressive cooling and crystallization until the magma eventually reaches sulfide saturation. However, triggering sulfide segregation might require a significant degree of crystallization and the magma may be as highly evolved as a ferrobasalt (e.g., Mungall and Naldrett, 2008). Li et al. (2012) suggested that fractional crystallization did not play a critical role in inducing sulfide saturation in the Emeishan basaltic magmas. In terms of the post-ELIP basalts, they are not so evolved because they have higher Cr contents (from 248 ppm to 648 ppm) than normal ferrobasalts (commonly less than 100 ppm, according to Iyer et al., 1999). If sulfide segregation did occur during fractional crystallization, the concentrations of PGE would drop dramatically. No such drop can be found in the Cr content and PGE are present in the post-ELIP basalts (Fig. 5b–f), which provides evidence that the

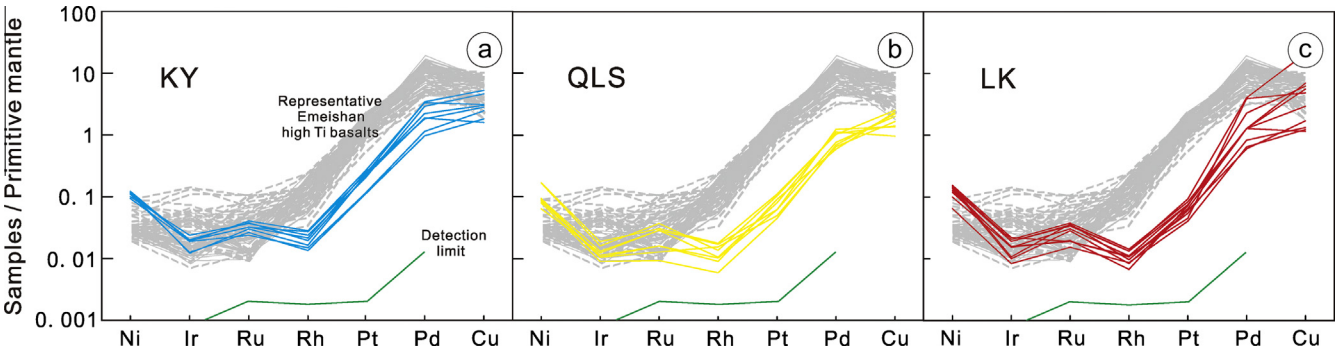

Fig. 4. Primitive mantle-normalized Ni–PGE–Cu patterns of basalts from the post-ELIP basalts. (a) The KY basalts; (b) the QLS basalts; (c) the LK basalts. The primitive mantle values for normalization are from Barnes and Maier (1999). The representive Emeishan high-Ti basalts data are from Wang et al. (2007), Qi et al. (2008), Qi and Zhou (2008), Song et al. (2008, 2009) and Li et al. (2012).

Table 3
Platinum-group element, S and other elements contents for the Anisian basalts, Kaiyuan and Gejiu areas.

Unit	Kaiyuan basalts								Qilinshan basalts				
Sample	11KY-2	11KY-3	11KY-4	11KY-5	11KY-6	11KY-8	11KY-10	11KY-11	QLS-1	QLS-2	QLS-6	QLS-7	QLS-8
Ir (ppb)	0.099	0.063	0.094	0.099	0.120	0.062	0.094	0.099	0.079	0.093	0.061	0.045	0.066
Ru (ppb)	0.127	0.106	0.094	0.127	0.144	0.119	0.163	0.153	0.148	0.122	0.113	0.037	0.113
Rh (ppb)	0.074	0.046	0.050	0.094	0.081	0.055	0.096	0.067	0.046	0.059	0.057	0.020	0.035
Pt (ppb)	1.700	0.779	0.802	1.638	1.431	1.560	1.812	1.518	0.715	0.759	0.427	0.314	0.551
Pd (ppb)	1.757	0.927	1.090	3.283	2.735	2.119	3.135	1.816	1.011	0.972	1.172	0.652	1.071
∑PGE (ppb)	3.756	1.921	2.130	5.242	4.511	3.916	5.300	3.653	1.999	2.005	1.831	1.068	1.836
S (ppm)	150	160	160	170	130	340	150	130	280	210	330	250	150
SCSS (ppm)[a]	1850	1882	2005	1820	1491	1852	1255	1747	1607	1881	1398	1517	1542
MgO (wt.%)[a]	11.5	9.97	11	10.4	7.84	10.3	6.46	8.83	10.5	11.3	7.49	9.8	10.6
Ni (ppm)[a]	231	222	242	241	203	239	186	223	336	333	129	161	182
Cu (ppm)[a]	77.9	51.4	67.8	148.5	131	84	86.8	44.6	39.1	69.5	38.3	62.1	27.1
Cr (ppm)[a]	404	401	417	279	260	459	305	408	647	648	248	289	333
Sm (ppm)[a]	7.47	8	8.42	7.75	7.6	7.54	6.54	7.19	5.16	5.33	8.45	7.3	7.73
Yb (ppm)[a]	1.57	1.46	1.42	1.52	1.54	1.62	1.47	1.46	1.39	1.45	1.55	1.94	1.6
$(Th/Nb)_N$[a]	0.91	0.98	0.95	1.09	1.01	1.19	0.87	0.88	0.76	0.75	0.75	0.66	0.74
$(Nb/La)_N$[a]	0.89	0.91	0.91	0.77	0.93	0.90	1.08	0.96	1.45	1.48	1.13	1.30	1.32
	Qilinshan basalts							Laoka basalts					
	QLS-9	QLS-10	QLS-11	KF-2	KF-6	KF-7	KF-8	LC-1	LC-2	LC-3	LC-4	LC-7	LC-8
Ir (ppb)	0.052	0.053	0.055	0.112	0.096	0.096	0.103	0.078	0.053	0.079	0.051	0.042	0.077
Ru (ppb)	0.051	0.062	0.064	0.077	0.138	0.133	0.152	0.079	0.147	0.075	0.114	0.060	0.122
Rh (ppb)	0.052	0.031	0.034	0.038	0.046	0.046	0.048	0.023	0.033	0.036	0.028	0.029	0.038
Pt (ppb)	0.346	0.640	0.437	0.321	0.649	0.520	0.582	0.509	0.461	0.376	0.419	0.280	0.516
Pd (ppb)	0.615	0.560	0.726	3.704	3.826	1.229	1.212	2.153	1.231	0.797	0.582	0.614	1.213
∑PGE (ppb)	1.116	1.346	1.316	4.251	4.755	2.024	2.098	2.842	1.925	1.363	1.194	1.025	1.966
S (ppm)	220	190	200	3460	2550	1130	2670	450	1490	2030	370	960	2710
SCSS (ppm)[a]	1561	1643	1546	1547	1450	1729	1976	1630	1772	1513	1645	1581	1513
MgO (wt.%)[a]	11.1	10.7	12.8	12.5	16.3	19.7	14.2	12	11.4	12.9	14.4	10.8	12.3
Ni (ppm)[a]	168	187	176	285	297	277	285	261	350	238	280	132	199
Cu (ppm)[a]	46.3	66.1	56.4	13.3	586	32.5	155	173	259	37.1	47.6	34.2	81.8
Cr (ppm)[a]	291	312	357	626	515	619	539	492	474	425	494	260	548
Sm (ppm)[a]	6.86	7.04	6.99	5.7	5.53	6.24	5.75	5.63	5.54	4.76	5.71	7.54	7.14
Yb (ppm)[a]	1.84	2	1.57	1.61	1.5	1.59	1.56	1.46	1.46	1.28	1.53	1.52	1.69
$(Th/Nb)_N$[a]	0.69	0.69	0.75	0.68	0.87	0.74	0.76	0.86	0.87	0.88	0.85	0.68	0.73
$(Nb/La)_N$[a]	1.39	1.22	1.27	1.43	1.04	1.35	1.38	1.33	1.28	1.21	1.19	1.50	1.25

[a] Zhang et al. (unpublished results).

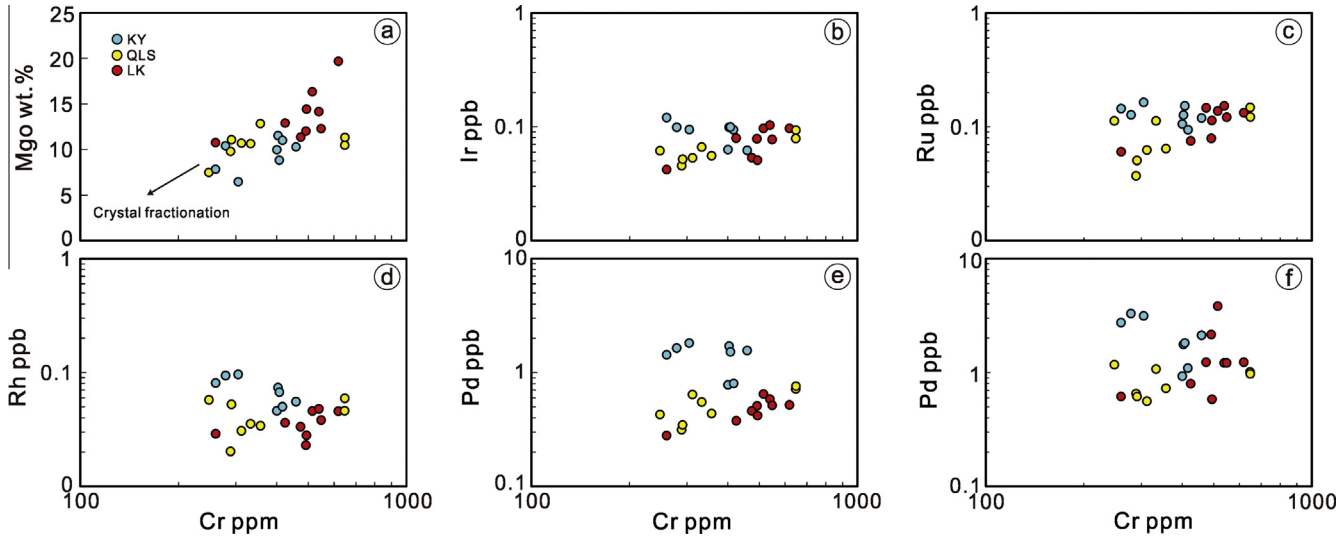

Fig. 5. Relationships between PGE contents and fractionation indexes (Cr content) for post-ELIP basalts.

sulfide segregation did not occur and the low PGE contents are not controlled by fractional crystallization.

The addition of cool crustal material can simultaneously increase the silica concentration and decrease the temperature, both of which conspire to hasten sulfide saturation and sulfide segregation (e.g., Mungall and Naldrett, 2008). $(Nb/La)_N$ and $(Th/Nb)_N$ ratios are good proxies for crustal contamination (Wang et al., 2007). As illustrated in Fig. 6a, the post-ELIP basalts did undergo crustal contamination, as indicated by the negative correlation between $(Nb/La)_N$ and $(Th/Nb)_N$. The KY basalts had suffered more crustal contamination than the QLS and LK basalts. However, Sr–Nd isotope model calculations indicate that only very small

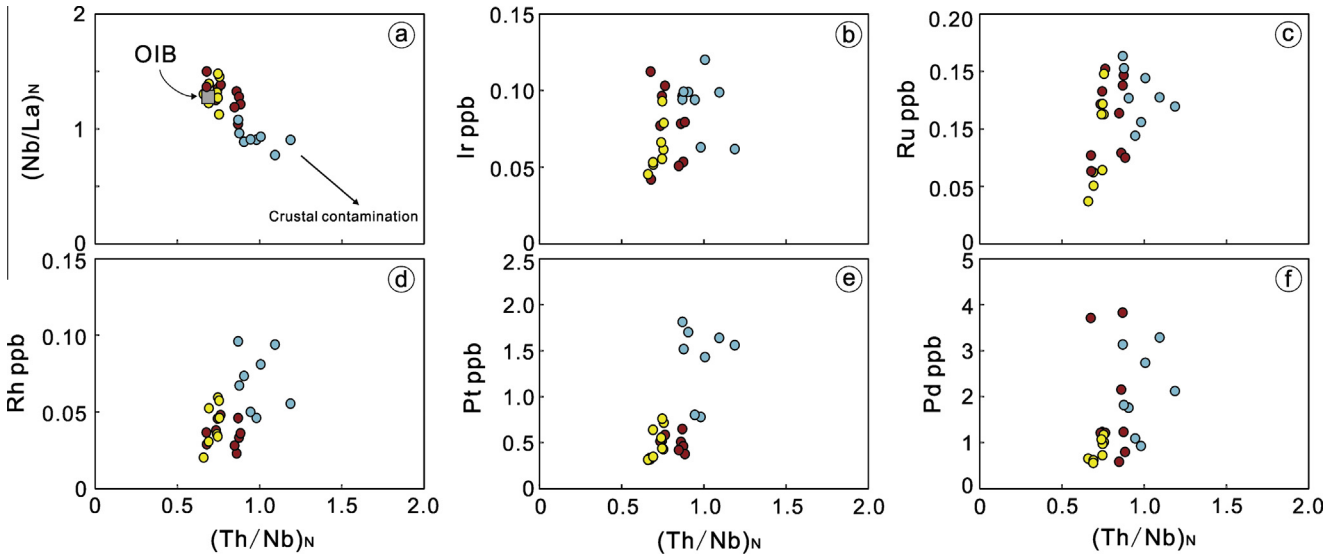

Fig. 6. Relationships between PGE contents and crustal contamination indexes $(Th/Nb)_N$ for post-ELIP basalts. The primitive mantle values are from McDonough and Sun (1995).

amounts of crustal materials (5–10% maximum) have been involved (Zhang et al., 2013, unpublished results). More importantly, the post-ELIP basalts show poor correlations between the $(Th/Nb)_N$ ratios versus PGE concentrations (Fig. 6b–f). If sulfide segregation was caused by crustal contamination, the KY basalts should have the lowest PGE contents compared with the QLS and LK basalts. As evident from Fig. 6b–f, no such trend could be observed. Therefore, no sulfide segregation has been triggered by crustal contamination in the post-ELIP basalts.

During magma's ascent from the mantle, the decrease in pressure will cause a dramatic increase in its ability to dissolve sulfur (Wendlandt, 1982; Mavrogenes and O'Neill, 1999; Naldrett, 2010). Thus even a magma that was saturated in sulfur when it left its source will be far from saturated on nearing the surface and hence cannot readily produce an immiscible sulfide phase for sulfide segregation. Therefore, the significant depletion of PGE in the post-ELIP basalts is controlled by a mechanism other than sulfide segregation from fractional crystallization or crustal contamination.

5.2. Low-degree partial melting

The base-metal sulfides in the upper mantle play a pivotal role in controlling PGE abundances in mantle-derived magmas (Morgan, 1986; Pattou et al., 1996; Burton et al., 2002; Luguet et al., 2007). Because PGE have sulfide melt/silicate melt partition coefficients of 10^3–10^6 (Ballhaus et al., 2006), as long as sulfides remain in the upper mantle during partial melting, magmas in equilibrium with sulfides remaining in the residual mantle will be PGE-poor and S-saturated. Magmas formed under these conditions have negligible PGE contents (Mungall and Naldrett, 2008). In contrast, magmas formed by a high degree of partial melting, i.e., beyond complete consumption of sulfides (e.g., Archean komatiites) are PGE-rich and S-undersaturated. As evident from Fig. 7a, the post-ELIP basalts are S-saturated basalts according to the division from Li et al. (2012).

The sulfur concentrations at sulfide saturation (SCSS) is controlled by the solubility of S in the silicate melt, which is defined at a given T, P, oxygen fugacity (fO_2) and major element composition of the melt. From the empirical equation of Li and Ripley (2009), the calculated sulfur concentrations at sulfide saturation (SCSS) of the magmas that produced the post-ELIP basalts range from 1255 to 2055 ppm, with an average of 1652 ppm. In our normative calculation, T = 1500 °C, P = 30 kbar (according to the melting condition of Emeishan basalts from Xu and Chung, 2001), no water is added, and the whole-rock FeO/Fe_2O_3 ratio of 0.9 was used.

The Cu, S and Pt + Pd contents of primary mantle-derived magmas could determined from melting models of garnet lherzolite by the method of Lee et al. (2012). Assumptions made in modeling are listed in Table 4 and the melting routine is provided as an Excel spreadsheet (Supplementary Tables S1 and S2). Making the common assumption that the mantle contains 200 ppm S (Lorand, 1990), the average SCSS of the post-ELIP basalts is 1652 ppm, by 13% melting, the sulfide present in the source will entirely dissolved in the silicate liquid (Fig. 7b). As the result from modeling, the silicate melt will have empirical Cu content of 127 ppm and Pt + Pd content of 10.4 ppb.

We used Sm and Sm/Yb ratios to constrain the degree of partial melting base the modeling of Aldanmaz et al. (2000). The modeling uses the non-modal batch melting equations of Shaw (1970) and the REE partition coefficient compilation of McKenzie and O'Nions (1991, 1995). The assumed mineralogy of garnet-lherzolite is 60% ol, 20% opx, 10% cpx and 10% garnet (Walter, 1998). The samples with high MgO (>8 wt.%) were selected to estimate the degree of partial melting because those may bear the information about the partial melting and source history. The early calculation (Zhang et al., 2013, unpublished results) shows that the post-ELIP basalts had experienced 4–12% partial melting, which is less than 13%. Besides, The average Cu content and Pt + Pd content of the post-ELIP basalts is 97 ppm and 2.32 ppb, which consistent with only 7% and 11% melting, respectively. Therefore, there is a high probability that most of the PGE still in the upper mantle reside in sulfides phases, causing the post-ELIP basalts to be strikingly depleted in PGE contents.

There are two sulfide populations in the mantle (Alard et al., 2000; Lorand et al., 2008): (1) Os–Ir–Ru-rich sulfides and (2) Pd- and Pt-rich intergranular Ni sulfide (pentlandite) and Cu sulfide (chalcopyrite–isocubanite). The former come in the form of rounded Fe–Ni monosulfide solid solution (MMS) inclusions in olivine. These sulfides display a negatively sloped chondrite-normalized PGE pattern. The second kind of sulfide exhibits a basalt-like, positively sloped chondrite-normalized PGE pattern. During low-degree partial melting, these latter sulfides have a

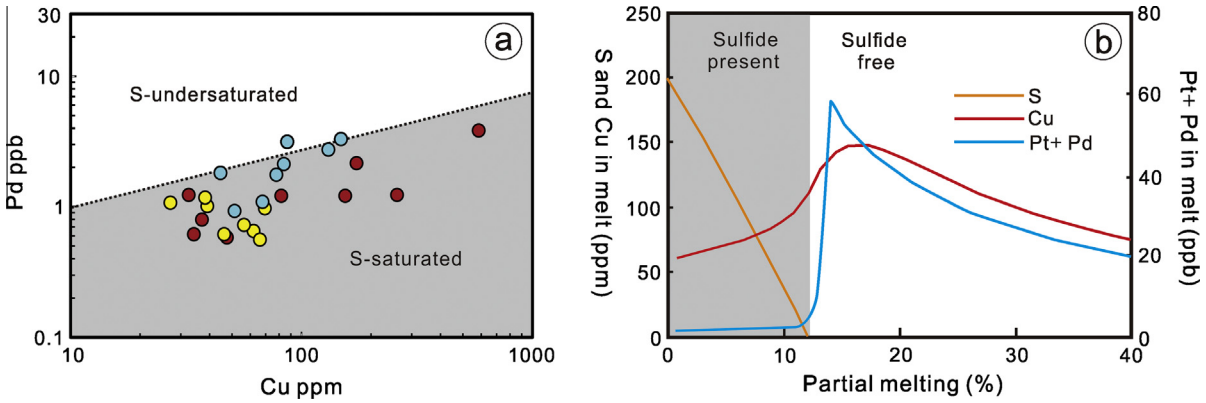

Fig. 7. (a) Plots of Pd versus Cu. The division for S-saturated and S-undersaturated basalts is from Li et al. (2012). (b) Sulfur in upper mantle residues remaining after varying degrees of partial melt extraction and the Cu, (Pt + Pd) content in melt. Note that melts formed by greater than 13% partial melting will totally deplete the mantle in S.

Table 4
Assumptions made in modeling.

The assumed mineralogy of mantle is from Walter (1998): 60% ol, 20% opx, 10% cpx, and 10% garnet and 0.06% sulfide. Mantle contents of S are from Lorand (1990) and Cu, Pt, Pd are from Crocket et al. (1992): S = 200 ppm; Cu = 30 ppm; Pt = 4 ppt; Pd = 4 ppb
Melting temperature and melting pressure are from Xu and Chung (2001): T = 1500 °C; P = 3.0 GPa. The assumed fO_2 value ΔFMQ = 0. No water. FeO/Fe_2O_3 = 0.9 was used. SCSS = 1652 ppm
Partition coefficients of Pt and Pd between Sulfide melt and Silicate melt are from Naldrett (2011): $D_{(Pt+Pd)}$ = 14,000; mineral/melt partition coefficients of Cu are from Lee et al. (2012): $D_{ol/melt}$ = 0.05; $D_{opx/melt}$ = 0.05; $D_{cpx/melt}$ = 0.05; $D_{garnet/melt}$ = 0.004; $D_{sulfide/silicate}$ = 800

low-melting-temperature. They will melt first whereas the former sulfides are still trapped in the mantle. Accordingly, the melt will be rich in Pd and Pt but depleted in Ir and Ru (Ballhaus et al., 2006). Lee (2002) reported high Pt, Pd and Cu in metasomatized peridotite xenoliths, suggesting those elements are strongly fractionated into sulfide liquids, whereas Ir, Ru, Rh are fractionated into sulfide solids.

Brenan et al. (2012) indicated that IPGE (especially Ru) strongly partition into spinel, with partition coefficients of 4–35 (D_{Ru}) between spinel and magma. The partition coefficients D_{Ru} between olivine and magma range from 0.23 to 1.7 (Righter et al., 2004; Puchtel and Humayun, 2001). However, As evident from Fig 5b and c, there are no correlations between Ir and Cr and between Ru and Cr, which indicates the IPGE depletion is not caused by the crystal fractionation of Cr-spinel and olivine. Consequently, the depletion of the IPGE relative to the PPGE in the primitive mantle–normalized elements diagrams of the post-ELIP basalts is due to the low degree of partial melting.

The empirical S content (1652 ppm) of melt is much higher than the measured S contents (130–340 ppm) of the whole-rock of KF and QLS samples. This is reasonable because S can partially to strongly degas to a vapor phase and be released during eruptions. As a result, the melt would have lost up to 90% of S via volatilization at the Earth's surface (Keays, 1995; Wallace and Edmonds, 2011). In contrast, the LK basalts, which are located close to the Gejiu Cretaceous Laochang granites, have suffered strong late-stage alteration, sulfide mineralization, and dolomite wall-rock alteration simultaneously (Zhang et al., unpublished results). These rocks may gain S from these processes, leading to an increase of their S contents.

5.3. PPGE depletion of post-ELIP basalts during early ELIP extraction

Only Permian Emeishan basalts are found in the Kaiyuan–Gejiu area (YBGMR, 1982), indicating that the mantle of this area had suffered low-degree melting during the Permian Emeishan magmatism. Because of the different sites of crystallization and contrasting mineralogical and geochemical compositions of the two types of sulfides in the mantle, the low-degree melting magmatism will lead to a mantle strongly depleted in PPGE without changing the contents of IPGE (e.g., Lorand et al., 2008) and the Emeishan basalts will have a positively sloped chondrite-normalized PGE pattern.

As shown in Fig. 4, the IPGE contents of the post-ELIP basalts are close to those of the Emeishan high-Ti basalts, whereas the PPGE contents are strikingly depleted. This is because, when the PPGE-depleted mantle suffers low-degree partial melting again during the Triassic, the melt (post-ELIP basalts) would also have positively sloped chondrite-normalized PGE patterns. The IPGE contents of the post-ELIP basalts would be consistent with the Emeishan basalts because both formed by low-degree partial melting (incomplete consumption of sulfides in the mantle, with IPGE still hosted in sulfides). However, the post-ELIP basalts are expected to have less PPGE contents than the Emeishan basalts owing to the early extraction of PPGE from the same mantle. Based on this discussion, we interpret the early extraction of PPGE to be the main reason for the PPGE depletion of the post-ELIP basalts.

6. Conclusions

Our study of the LA-ICP-MS dating and PGE concentrations of the post-ELIP basalts lead to the following conclusions:

(1) The new LA-ICP-MS dating result yields an age of 247.7 ± 1.4 Ma for the KY volcanic rocks, which is almost 10 Ma younger than the termination age of the ELIP magmatism. The KY, QLS, and LK basalts are a proxy for post-ELIP magmatism.
(2) The low PGE contents of the post-ELIP basalts are not attributed to sulfide segregation caused by fractional crystallization or crustal contamination, whereas it could be the result of low-degree partial melting of mantle source.
(3) The striking PPGE depletion of the post-ELIP basalts is considered to be caused by the early extraction of PPGE during the eruption of the Emeishan basalts.

(4) During its ascent, the primary S-saturated melt became S-undersaturated because of the decrease in pressure. The measured S contents are lower than the empirical SCSS because S was lost to a vapor phase during the eruption of the basalts, causing a decoupling between PGE concentrations and S contents.

Acknowledgements

We thank Yan Tao, Dan Zhu for their help and constructive discussions. Liang Qi and Yifan Yin is thanked for the PGE determinations. The manuscript was improved by constructive and helpful reviews from Hong Zhong and Lin Ye. Professor Cin-Ty Aeolus Lee and another anonymous referees is grateful for critical reading of the manuscript. This study was financially supported by the Crisis Mines Continued Resources Exploration Project of the China Geological Survey (No. 2008186), the 12th Five-Year Plan project of the State Key Laboratory of Ore-deposit Geochemistry, the Chinese Academy of Sciences (SKLODG-ZY125-02) and the National Natural Science Foundation of China (No. 41073032) and the geochemical research of high strength-field element on Ertan basalts in Emeishan large igneous province, China (No. 41103024).

Appendix A. Supplementary material

Supplementary data associated with this article can be found, in the online version, at http://dx.doi.org/10.1016/j.jseaes.2014.02.023.

References

Alard, O., Griffin, W.L., Lorand, J.-P., Jackson, S.E., O'Reilly, S.Y., 2000. Non-chondritic distribution of the highly siderophile elements in mantle sulphides. Nature 407, 891–894.

Aldanmaz, E., Pearce, J.A., Thirlwall, M.F., Mitchell, J.G., 2000. Petrogenetic evolution of late Cenozoic, post-collision volcanism in western Anatolia, Turkey. J. Volcanol. Geoth. Res. 102, 67–95.

Ballhaus, C., Bockrath, C., Wohlgemuth-Ueberwasser, C., Laurenz, V., Berndt, J., 2006. Fractionation of the noble metals by physical processes. Contrib. Miner. Petrol. 152, 667–684.

Barnes, S.-J., Maier, W.D., 1999. The fractionation of Ni, Cu, and the noble metals in silicate and sulfide liquids. Geol. Assoc. Can. Short Course Notes 13, 69–106.

Barnes, S.J., Naldrett, A.J., Gorton, M.P., 1985. The origin of the fractionation of platinum-group elements in terrestrial magmas. Chem. Geol. 53, 303–323.

Brenan, J.M., Finnigan, C.F., McDonough, W.F., Homolova, V., 2012. Experimental constraints on the partitioning of Ru, Rh, Ir, Pt and Pd between chromite and silicate melt: the importance of ferric iron. Chem. Geol. 302–303, 16–32.

Burton, K.W., Gannoun, A., Birck, J.-L., Allegre, C.J., Schiano, P., Clocchiatti, R., Alard, O., 2002. The compatibility of rhenium and osmium in natural olivine and their behavior during mantle melting and basalt genesis. Earth Planet. Sci. Lett. 198, 63–76.

Cheng, Y.B., Mao, J.W., 2010. Age and geochemistry of granites in Gejiu area, Yunnan Province, SW China: constraints on their petrogenesis and tectonic setting. Lithos 120, 258–276.

Chung, S.-L., Jahn, B.-M., 1995. Plume–lithosphere interaction in generation of the Emeishan flood basalts at the Permian–Triassic boundary. Geology 23, 889–892.

Crocket, J.H., Fleet, M.E., Stone, W.E., 1992. Experimental partitioning of osmium iridium and gold between basalt melt and sulfide liquid at 1300 °C. Aust. J. Earth Sci. 39, 427–432.

Fleet, M.E., Crocket, J.H., Liu, M., Stone, W.E., 1999. La boratory partitioning of platinum-group elements (PGE) and gold with application to magmatic sulfide-PGE deposits. Lithos 47, 127–142.

Govindaraju, K., 1994. Compilation of working values and sample description for 383 geostandards. Geostandards Newslett. 18 (2), 1–158.

He, B., Xu, Y.G., Huang, X.L., Luo, Z.Y., Shi, Y.R., Yang, Q.J., Yu, S.Y., 2007. Age and duration of the Emeishan flood volcanism, SW China: geochemistry and SHRIMP zircon U–Pb dating of silicic ignimbrites, post-volcanic Xuanwei Formation and clay tuff at the Chaotian section. Earth Planet. Sci. Lett. 255, 306–323.

Iyer, S.D., Mukhopadhyay, R., Popko, D.C., 1999. Ferrobasalts from the Central Indian Ocean Basin. Geo-Mar. Lett. 18, 297–323.

Keays, R.R., 1995. The role of komatiitic and picritic magmatism and S-saturation in the formation of ore deposits. Lithos 34, 1–18.

Lee, C.-T.A., 2002. Platinum-group element geochemistry of peridotite xenoliths from the Sierra Nevada and the Basin and Range, California. Geochim. Cosmochim. Acta 66, 3987–4005.

Lee, C.-T.A., Luffi, P., Chin, E.J., Bouchet, R., Dasgupta, R., Morton, D.M., Le Roux, V., Yin, Q.Z., Jin, D., 2012. Copper systematics in arc magmas and implications for crust–mantle differentiation. Science 336, 64–68.

Li, C.S., Ripley, E.M., 2009. Sulfur contents at sulfide-liquid or anhydrite saturation in silicate melts: Empirical equations and example applications. Econ. Geol. 104, 405–412.

Li, Z.X., Wartho, J.A., Occhipinti, S., Zhang, C.L., Li, X.H., Wang, J., Bao, C.M., 2007. Early history of the eastern Sibao orogen (South China) during the assembly of Rodinia: new $^{40}Ar/^{39}Ar$ dating and U–Pb SHRIMP detrital zircon provenance constraints. Precambr. Res. 159, 74–94.

Li, C., Tao, Y., Qi, L., Ripley, E.M., 2012. Controls on PGE fractionation in the Emeishan picrites and basalts: constraints from integrated lithophile–siderophile elements and Sr–Nd isotopes. Geochim. Cosmochim. Acta 90, 12–32.

Lightfoot, P.C., Keays, R.R., 2005. Siderophile and chalcophile metal variations in flood basalts from the Siberian Trap, Noril'sk Region: implications for the origin of the Ni–Cu–PGE sulfide ores. Econ. Geol. 100 (3), 439–462.

Liu, Y.S., Hu, Z.C., Zong, K.Q., Gao, C.G., Gao, S., Xu, J., Chen, H.H., 2010a. Reappraisement and refinement of zircon U–Pb isotope and trace element analyses by LA-ICP-MS. Chin. Sci. Bull. 55 (15), 1535–1546.

Liu, Y.S., Gao, S., Hu, Z.C., Gao, C.G., Zong, K.Q., Wang, D.B., 2010b. Continental and oceanic crust recycling-induced melt-peridotite interactions in the Trans-North China Orogen: U–Pb dating, Hf isotopes and trace elements in zircons from mantle xenoliths. J. Petrol. 51 (1–2), 537–571.

Lorand, J.P., 1990. Are spinel lherzolite xenoliths representative of the abundance of sulfur in the upper mantle? Geochim. Cosmochim. Acta 54, 1487.

Lorand, J.P., Luguet, A., Alard, O., 2008. Platinum-group elements: a new set of key tracers for the Earth's interior. Elements 4 (4), 247–252.

Ludwig, K.R., 2003. ISOPLOT 3.0: A Geochronological Toolkit for Microsoft Excel. Berkeley Geochronology Center Special Publication, 4, 71 p.

Luguet, A., Shirey, S.B., Lorand, J.-P., Mary, F., Horan, M.F., Richard, W., Carlson, R.W., 2007. Residual platinum-group minerals from highly depleted harzburgites of the Lherz massif (France) and their role in HSE fractionation of the mantle. Geochim. Cosmochim. Acta 71 (12), 3082–3097.

Luo, R.S., Yang, X.S., Zhang, S.Y., Wang, W.X., 2008. Lithofacies and paleogeographic conditions for Gejiu cassiterite bearing sulfides deposit, Yunnan. Geol. Prospect. 44, 36–41 (in Chinese with English abstract).

Mavrogenes, J.A., O'Neill, H.S.C., 1999. The relative effects of pressure temperature and oxygen fugacity on the solubility of sulfide in mafic magmas. Geochim. Cosmochim. Acta 63, 1173–1180.

McDonough, W.F., Sun, S.-S., 1995. The composition of the Earth. Chem. Geol. 120, 223–253.

McKenzie, D.P., O'Nions, R.K., 1991. Partial melt distribution from inversion of rare earth element concentrations. J. Petrol. 32, 1021–1991.

McKenzie, D.P., O'Nions, R.K., 1995. The source regions of ocean island basalts. J. Petrol. 36, 133–159.

Metcalfe, I., 2006. Palaeozoic and Mesozoic tectonic evolution and palaeogeography of East Asian crustal fragments: the Korean Peninsula in context. Gondwana Res. 9, 24–46.

Morgan, J.W., 1986. Ultramafic xenoliths: clues to the Earth's late accretionary history. J. Geophys. Res. 91 (B12), 12375–12387.

Mungall, J.M., Naldrett, A.J., 2008. Ore deposits of the platinum-group elements. Elements 4, 253–258.

Naldrett, A.J., 2010. From the mantle to the bank: the life of a Ni–Cu–(PGE) sulfide deposit. S. Afr. J. Geol. 113 (1), 1–32.

Naldrett, A.J., 2011. Fundamentals of magmatic sulfide deposits. Rev. Econ. Geol. 17, 1–50.

Pattou, L., Lorand, J.-P., Gros, M., 1996. Non-chondritic platinum-group element ratios in the Earth's mantle. Nature 379, 712–715.

Puchtel, I., Humayun, M., 2001. Platinum group element fractionation in a komatiitic basalt lava lake. Geochim. Cosmochim. Acta 65, 2979–2993.

Qi, L., Zhou, M.-F., 2008. Platinum-group elemental and Sr–Nd–Os isotopic geochemistry of Permian Emeishan flood basalts in Guizhou Province, SW China. Chem. Geol. 248, 83–103.

Qi, L., Wang, C.Y., Zhou, M.-F., 2008. Controls on the PGE distribution of Permian Emeishan alkaline and peralkaline volcanic rocks in Longzhoushan, Sichuan Province, SW China. Lithos 106, 222–236.

Qi, L., Gao, J., Huang, X., Hu, J., Zhou, M.-F., Zhong, H., 2011. An improved digestion technique for determination of platinum group elements in geological samples. J. Anal. Atom. Spectrom. 26 (9), 1900–1994.

Righter, K., Campbell, A.J., Humayun, M., Hervig, R.L., 2004. Partitioning of Ru, Rh, Pd, Re, Ir, and Au between Cr-bearing spinel, olivine, pyroxene and silicate melts. Geochim. Cosmochim. Acta 68 (4), 867–880.

Shaw, D.M., 1970. Trace element fractionation during anatexis. Geochim. Cosmochim. Acta 34, 237–243.

Shellnutt, J.G., Denyszyn, S.W., Mundil, R., 2012. Precise age determination of mafic and felsic intrusive rocks from the Permian Emeishan large igneous province (SW China). Gondwana Res. 12, 118–126.

Song, X.-Y., Qi, H.-W., Robinson, P.T., Zhou, M.-F., Cao, Z.-M., Chen, L.-M., 2008. Melting of the subcontinental lithospheric mantle by the Emeishan mantle plume; evidence from the basal alkaline basalts in Dongchuan, Yunnan, Southwestern China. Lithos 100, 93–111.

Song, X.-Y., Keays, R.R., Xiao, L., Qi, H.-W., Ihlenfeld, C., 2009. Platinum-group element geochemistry of the continental flood basalts in the central Emeisihan Large Igneous Province, SW China. Chem. Geol. 262, 246–261.

Wallace, P.J., Edmonds, M., 2011. The sulfur budget in magmas: evidence from melt inclusions, submarine glasses, and volcanic gas emissions. Rev. Mineral. Geochem. 73 (1), 215–246.

Walter, M.J., 1998. Melting of garnet peridotite and the origin of komatiite and depleted lithosphere. J. Petrol. 39 (1), 29–60.

Wang, C.Y., Zhou, M.-F., Qi, L., 2007. Permian basalts and mafic intrusions in the Jinping (SW China)-Song Da (northern Vietnam) district: mantle sources, crustal contamination and sulfide segregation. Chem. Geol. 243, 317–343.

Wendlandt, R.F., 1982. Sulfur saturation of basalt and andesite melts at high pressures and temperatures. Am. Mineral. 67, 877–885.

Xu, Y.G., Chung, S.L., 2001. The Emeishan Large Igeneous Province: evidence for mantle plume activity and melting conditions. Geochimica 30 (1), 1–9 (in Chinese with English abstract).

Xu, Y.G., Chung, S.L., Jahn, B.M., Wu, G.Y., 2001. Petrologic and geochemical constraints on the petrogenesis of Permian–Triassic Emeishan flood basalts in southwestern China. Lithos 58, 145–168.

Xu, Y.-G., He, B., Chung, S.L., Menzies, M.A., Frey, F.A., 2004. Geologic, geochemical, and geophysical consequences of plume involvement in the Emeishan flood-basalt province. Geology 32 (10), 917.

Xue, C.D., 2002. The Space-Time Structure Model of the Gejiu Super Large Tin–Copper–Polymetallic Deposit. Dissertation, Kunming University of Science and Technology, China (in Chinese with English abstract).

YBGMR (Yunnan Bureau of Geology and Mineral Resources), 1982. Regional Geology of Yunnan Province. Geological Publishing House, Beijing (in Chinese with English abstract).

Zhang, J., Mao, J.W., Cheng, Y.B., Li, X.L., 2012. ^{40}Ar–^{39}Ar isotope age study of phlogopite from Kafang altered basalt in Gejiu of Yunnan Province and its significance. Geol. China 39 (6), 1647–1656.

Zhang, J., Huang, Z., Luo, T., Qian, Z., Zhang, Y., 2013. Origin of Early Triassic rift-related alkaline basalts from SW China: age, isotope and trace-element constraints. Int. Geol. Rev. 55, 1162–1178.

Zheng, R.C., Liu, W.J., 1993. The volcanic rocks and tectonic environments during hercynian–indosinian stage in Ailao mountain and western Youjiang. J. Chengdu College Geol. 20, 10–23 (in Chinese).

Zhou, M.F., Malpas, B., Song, C., Robinson, P.T., Sun, M., Kennedy, A.K., Lesher, C.M., Keays, R.R., 2002. A temporal link between the Emeishan large igneous province (SW China) and the end-Guadalupian mass extinction. Earth Planet. Sci. Lett. 196, 113–122.